AMBER

The imaging and spectroscopic VLTI focal instrument

F. Malbet (Observatoire de Grenoble),
G. Perrin (Observatoire de Paris-Meudon),
R. Petrov (Université de Nice),
A. Richichi (Osservatorio Astrofisico di Arcetri),
M. Schöller (Max-Planck-Institut für Radioastronomie, Bonn)

July 9, 1997

Abstract

We have studied a concept for an imaging and spectroscopic focal instrument for VLTI, AMBER[1]. This instrument complies with the ISAC 1996 recommendations [1], the revised ESO implementation plan [2] and the tripartite agreement [3].

The identified primary science objectives are:

- study of the inner 1 parsec of active galactic nuclei
- direct detection of massive extrasolar planets
- study of the circumstellar environment in star forming regions
- multiple objects, fundamental stellar astrophysics

The main characteristics of this instrument are:

- design of a 3-way beam combiner
- spatial filtering and accurate visibility calibration
- high optical throughput thanks to adaptive optics
- early operation with 2 UTs in 2000 in the near-infrared (1-2.5 μm)
- spectral resolution up to 10000
- spectral extension toward the red when ATs will be available (0.6-2.5 μm)

This report reviews the scientific and technical requirements of the instrument (chapter 1), the optical concept of the beam combiner (chapter 2), the list of instrument subsystems (chapter 3) and observing procedures and data reduction needs (chapter 4). Chapter 5 presents the anticipated performance of AMBER.

[1] Astronomical Multiple BEam Recombiner

Contents

List of Figures

List of Tables

Chapter 1

Scientific and technical requirements

1.1 Science objective and key projects

The science objectives for the instrument will be an important subset of the science drivers for the VLTI [1, 4], selected in consideration of the wavelength coverage, field of view, imaging capabilities and fringe tracking options.

The wavelength coverage will be limited initially to the near infrared (1 to 2.5 μm), although extensions to the red part of the visible spectrum are also foreseen (cf. Sect. 2.4). The field of view will vary from the size of an Airy disk (i.e., $\approx 0''.06$ at 2 μm for the UTs, or $\approx 0''.25$ for the ATs) to about $2''$ in the so-called "wide–field" mode. Although in the beginning only three baselines will be available simultaneously (number of Coudé trains in the ESO Phase-A/B Project [2]), the imaging instrument will be the only instrument for the VLTI to offer closure phase and thus, in principle, imaging capabilities. Such imaging will be more effective for simple sources, while objects with a complicated structure will require many telescope relocations and will be time consuming. Finally, the absence of phase referencing in a second beam will limit in practice fringe tracking to the science object itself. Limiting magnitudes will depend strongly on the bandpass of the selected filter and the color of the source, and on the AT/UT combination. Broadly speaking, one can think of a limiting magnitude $K \approx 10$ for the ATs, and $K \approx 13$ for the UTs [6]. However, note that several modes of operation are foreseen (see Sect. 1.3), including the so–called blind tracking which will allow to push the limiting magnitude somehow.

With these constraints in mind, we identify the following as some of the main science objectives for the instrument:

- Exoplanets (detecting hot massive Jupiters, i.e. such as 51 Peg)
- Star forming regions (disks and jets around young stellar objects)
- Circumstellar matter (circumstellar matter around AGB stars)
- AGN dust tori (probing the central engine by reprocessed radiation)
- Binaries (main sequence and giant stars, brown dwarfs, etc.)
- Stellar structure (limb–darkening, spots, rotation, etc.)

The actual scientific drivers for each of these issues have been described already in other documents, and we think that it is not necessary to present here a lengthy description of

Table 1.1: Scientific requirements for the imaging instrument.

Topic	Visib. Accur.	Limit Magn.	Wavelength Coverage	Spectr. Resol.	Polar-izat.	Wide Field	N_B	#2	#3
Exoplanets	10^{-4}	K>5	K	50	N	N	2	Y	Y
Star Forming Regions	10^{-2}	K>7	JHK+lines	1000	Y	Y	3	N	Y
Circumstellar matter	10^{-2}	K>4	JHK+lines	1000	Y	Y	3	N	Y
AGN dust tori	10^{-2}	K>11	K	50	Y	Y	3	N	Y
Binaries	10^{-3}	K>4	K	50	N	Y	2	Y	N
Stellar Structure	10^{-4}	K>1	lines	10000	N	N	3	N	N

N_B: Number of input beams, #2: astrometric instrument, #3: 10 μm instrument

each of these topics. The interested reader can find relevant information for instance in [1, 2, 3, 4, 5, 6]. More to the point of the present document, we summarize in Table 1.1 the requirements that each of the topics above imposes in the design of the instrument and the performance that it must achieve. We also have marked in the last two columns whether each field of research will constitute or not a primary science driver also for the other two instruments currently proposed for the VLTI, namely the astrometric instrument and the 10 μm instrument.

The values in the table should be interpreted as minimum requirements needed to carry out useful research in that field.

1.2 Main optical elements

The imaging and spectroscopic instrument contains a number of mandatory optical elements:

- adaptive optics
- fringe tracker
- cooled spectrograph
- 3-way beam combiner
- spatial filtering and photometric calibration
- polarization control with a Babinet prism
- near-infrared detector, and later, visible detector

These optical elements are required by the scientific objectives listed above. For example, spatial filtering and photometric calibration ensure visibility calibration better than 0.1% as needed for massive exoplanet study [7]. However such an optical scheme would be inefficient with $D/r_0 > 6$ and that is why adaptive optics is highly recommended. Fringe tracking is also mandatory when one wants to get high spectral resolution from interferometric data. Finally the aim of this instrument is to get images at very high angular resolution which requires phase closure measurements. The domain of operation will first be limited to the near infrared domain where the atmospheric disturbance is less important than in the visible range.

These elements will be described in more details in chapter 3.

Table 1.2: Instrument operating modes.

Instrument modes	Visib. Accur.	Wavelength Coverage	Spectr. Resol.	Polar- izat.	Wide Field	N_B	Science targets
Imaging	10^{-2}	JHK+lines	1000	Y	Y	≥ 3	AGNs, YSOs, Circ. Med.
High Precision Visibility	10^{-4}	K	50	N	N	2	Exoplanets, Binaries
High Spectral Resolution	10^{-3}	lines	10000	N	N	≥ 3	Stellar Structure

1.3 Main operating modes

1.3.1 Instrument modes

We have identified 3 instrument modes for the different scientific targets:

Imaging Mode (IM). It will be dedicated to the study of relatively complex spatial structures with a visibility accuracy of about 1%. Recombination of several beams is desirable in order to increase the (u, v) coverage. This mode should also allow us to push the performance of the instrument in sensitivity.

High Precision Visibility Mode (HPVM). It is foreseen for high dynamic range study of relatively simple objects, like multiple systems or massive hot Jupiters around stars. The goal is to have the most accurate calibration procedure as possible.

High Spectral Resolution Mode (HSRM). The high spectral resolution is recommended for the study of stellar lines. The spectral resolution is emphasized even if the accuracies in visibilities or the sensitivity performance are not extreme.

These operating modes are summarized in Table 1.2 together with the scientific requirements.

1.3.2 Acquisition modes

The choice of operation mode depends mostly on the tracking accuracy of the fringe sensor unit and thus on the brightness of the observed object. Figure 1.1 shows the different regimes.

- If the central fringe can be tracked by a fraction of a wavelength, say $\lambda/20$, we are in cophasing mode and can record long exposures up to the maximum integration time given by the longest baseline of the array and the wavelength used. In this regime the contrast loss is very low, e.g. 5×10^{-3} for a fringe tracking accuracy of $\lambda/20$.
- If the fringe tracking accuracy is better than $\lambda/2$, we are still in cophasing mode, but are encountering severe contrast loss (here: 0.37). It is still possible to make long exposures and use a linear estimator to retrieve visibilities.
- For even fainter objects the fringe sensor unit can't find the central fringe and hold it, but it may still be possible to control the envelope of the fringe packet. In this regime the fringe tracking accuracy is up to a few λ and

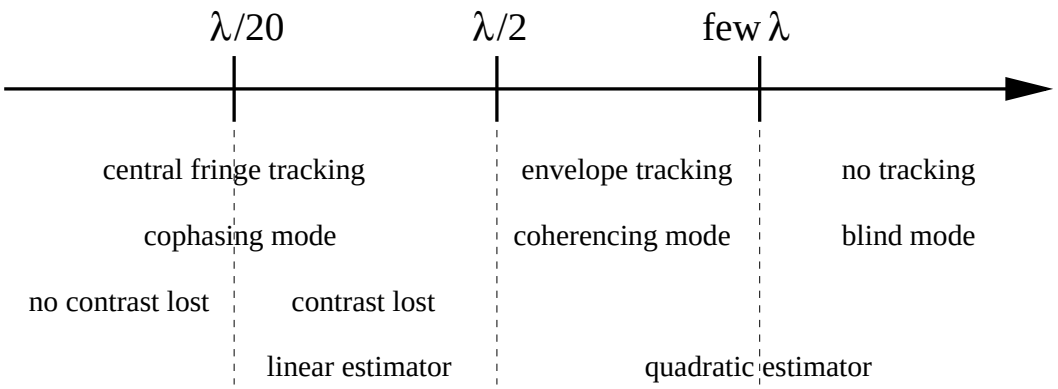

Figure 1.1: Fringe tracking accuracy. Overview about the fringe tracking regimes and the resulting acquistion modes.

one obtains short exposures, which have to be processed with a quadratic estimator to retrieve object information[1].

- If the fringe sensor isn't giving a reliable signal anymore, one has to observe in blind mode and scan the fringes. In this mode also short exposures are recorded and processed with a quadratic estimator.

1.4 Extension capabilities

The imaging and spectroscopic instrument should develop in different progressive stages. Even if it offers a 3-way beam combiner, the instrument will start by combining only two beams. Features described in chapter 3 are the nominal functions of the instrument. However one can wish to extend the capibility of the instrument in a more or less distant future:

Wavelength coverage. Extension to shorter wavelengths is foreseen when ATs will be operational. Adaptive optics will allow extension downward 0.6 μm with ATs. Extension to longer wavelengths (up to 5 μm) is also possible.

4-way beam combiner. With 2 UTs, 2 ATs, 3 active delay lines and a passive one, one can combine 4 beams. This will increase the number of baselines for which we can measure visibilities simultaneously.

Double feed. Telescopes will be equiped with double star feed for the astrometric instrument. Tracking the fringes and correcting the wavefronts on a separate reference star will improve the sensitivity of the instrument.

Extended adaptive optics. The sensitivity of the instrument is driven by the AO correction. Therefore increase of the degree of AO correction is wished as a long term goal.

[1] In this regime another operation mode is possible. Instead of trying to observe many short exposures at a more or less well known position, one slowly scans through the fringe pattern. Within a coherencing time exactly one fringe is scanned.

Coupling with other instruments. The interface with other instruments is desirable. For example, the imaging instrument can provide fringe sensing in the NIR domain for the 10 μm instrument.

Chapter 2

Optical concept

2.1 Two schemes for beam combination

The previous report [6] has presented different schemes for the instrument. Two major concepts have been selected: coaxial combination and multiaxial combination. The main differences are in the way fringes are detected.

2.1.1 Coaxial combination

The coaxial concept for the instrument is shown in Fig. 2.1. The beams are combined 2 by 2 with beamsplitters on the same axis. To measure the fringe signal, the optical path difference in each beam is modulated thanks to a mirror mounted on a piezo. The algorithm to measure the visibility and the phase are either the ABCD algorithm like in MarkIII or PTI [10], or, the exploration of the entire interferogram like in FLUOR [7]. The number of pixels needed for the configuration is discussed in the next section. This concept has been used in many existing instruments like MarkIII [10] and FLUOR on IOTA [7]. With the photometry calibration and perfect spatial filtering the visibility accuracy is excellent. To get spectral resolution, one needs to use optical fibers to feed the spectrograph since the size and the location of the beam in bulk optics would lead to a spectrograph too large (8m focal length!).

2.1.2 Multiaxial combination

The multiaxial optical concept for the instrument is shown in Fig. 2.2. The beams are combined together on the same plane. The pupil is a linear non-redundant array, which produces an Airy pattern with aligned fringes in the image. The direction perpendicular to the pupil elongation does not need the same sampling as the previous direction. Therefore a set of two cylindrical mirrors compresses the beam to obtain a compressed Airy pattern with fringe modulation. The distance between the fringes is directly linked to the pupil geometry. More fringes are obtained if the sub-pupils are moved away from each others. With the most compact pupil, one gets the measurements for one fringe. It is then necessary to create OPDs to measure the entire interferogram. This set-up is used by GI2T in the visible channel, but in multi-speckle mode. The fringe line can be used as the entrance slit of a conventional spectrograph[1].

[1] The beams are single-mode, therefore one does not have to sample the seeing disk and the spectrograph is much smaller than conventional spectrographs.

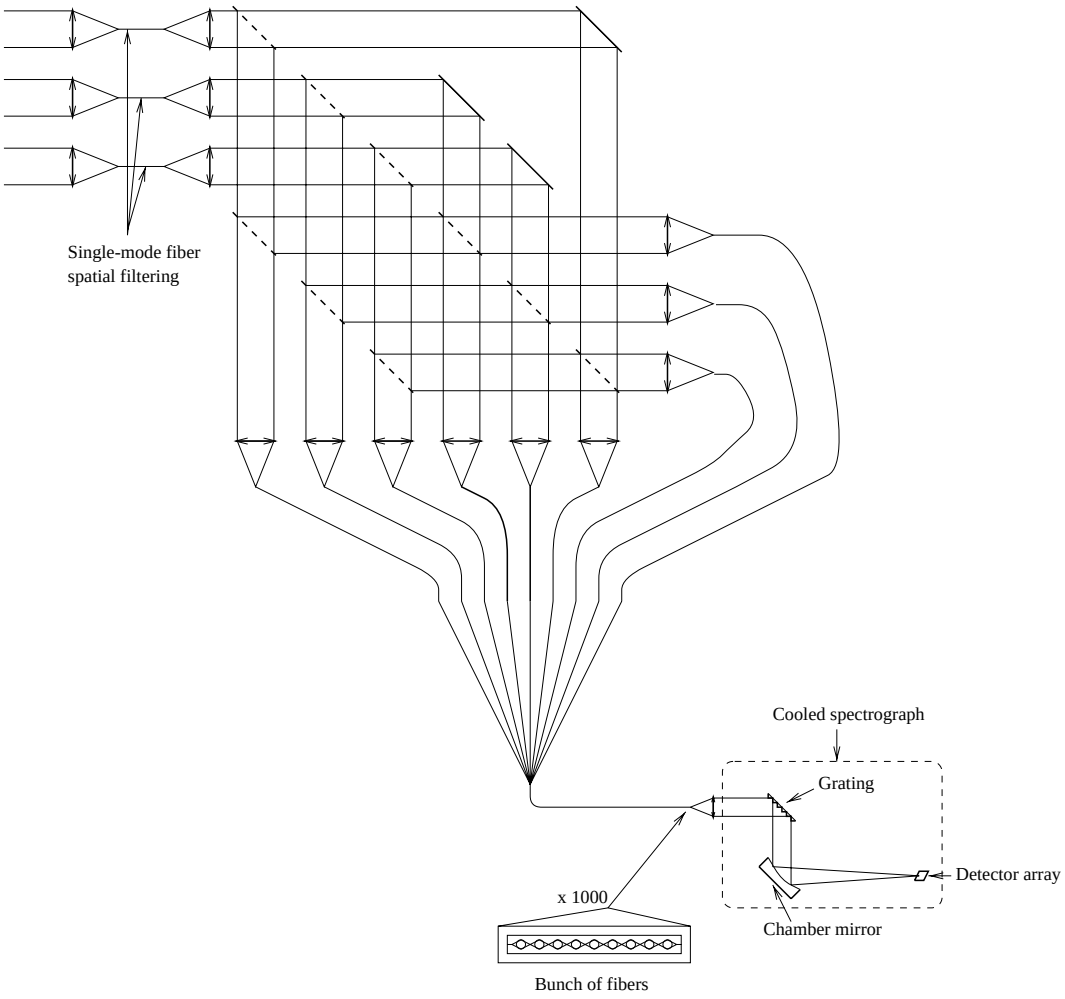

Figure 2.1: Coaxial optical concept.

2.2 Signal to noise ratio

It is intuitive that the number of pixels needed to measure the signal is about the same between the two schemes. In this section, we compare the signal to noise ratio (SNR) between the coaxial and the multiaxial configurations.

2.2.1 Cophasing mode

In cophasing mode, a fringe tracker ensures that the fringes do not move on the detector. With the coaxial recombination, one has to sample the central fringe with temporal modulation. With the multiaxial recombination, the sampling is done spatially and therefore no temporal modulation is necessary.

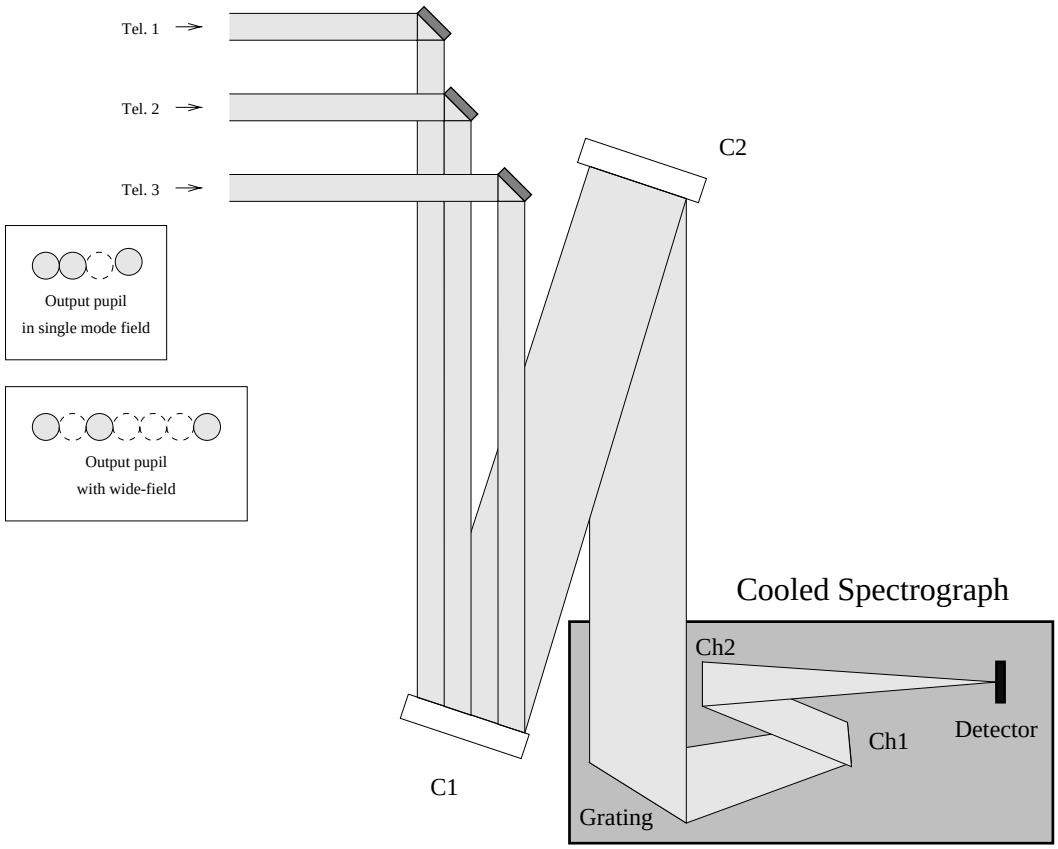

Figure 2.2: Multiaxial optical concept.

2.2.2 Coherencing mode

We have chosen the FLUOR-like acquisition mode to compare the performance of the two concepts. It consists in a fast scan of the entire interferogram. A fringe pattern containing N fringes is scanned in a time T of the order of the coherence time. The visibility estimator is the one developed on FLUOR.

The wavelengths are in the range $[\lambda_{\min}, \lambda_{\max}]$ with $\lambda_0 = (\lambda_{\max} + \lambda_{\min})/2$. One takes $\lambda_{\min} = 1.9$ μm, $\lambda_{\max} = 2.5$ μm and $\lambda_0 = 2.2$ μm. Typically $N \approx 10$ for the narrowest fringes in K band (for $\lambda_{\min}$).

2.2.2.1 Two telescopes

Coaxial recombination. The Nyquist "pixel" size is $\lambda_{\min}/2$ and we need $2N$ measurements in a time T for each of the output beams. Then the total number of measurements is:

- $4N$ measurements
- $\tau = T/2N$ elementary exposure time

All the flux is collected and if the modulation function has a staircase shape, there is no instrumental loss of contrast (for the $T/2N$ very short exposure time).

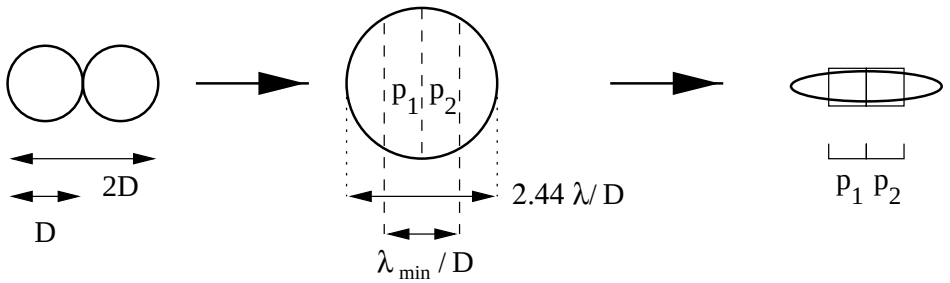

Figure 2.3: Number of pixels at a given time with 2 telescopes with the multiaxial scheme.

Multiaxial recombination. Figure 2.3 shows that the number of pixels at a given time is two. Therefore the fringe pattern is scanned by $2N$ steps of $\lambda_{\min}/2D$ size. The Nyquist pixel size is $p_x = \lambda_{\min}/2D$. We use the two central pixels of width $\lambda_{\min}/2D$ in an Airy pattern of size $2.44\lambda_0/D$. We then build a signal containing the $2N$ fringes by scanning the OPD by $2N$ steps of $\lambda_{\min}/2$. We have the same signal as in the coaxial case, but:

1. We lose about 30% of the flux at λ_0 because we do not use the edges of the Airy pattern
2. Due to the finite extension of the pixels (in fringe units) the fringe peak is multiplied by $\mathrm{sinc}(\lambda_{\min}/2\lambda)$, i.e.

   $\times 0.64$ for $\lambda_{\min}$
   $\times 0.72$ for λ_0
   $\times 0.78$ for $\lambda_{\max}$

For λ_0, the gain in signal with regard to the coaxial case is: $0.7 \times 0.72 = 0.5$. Therefore the gain in SNR is

$$\frac{\mathrm{SNR_{ca}}}{\mathrm{SNR_{ma}}} = 2 \tag{2.1}$$

Remarks

The optical throughput of the multiaxial setup is higher. In the April report [6], the multiaxial throughput is $t_{\mathrm{ma}} = 0.58$ and the coaxial throughput is $t_{\mathrm{ca}} = 0.48$. Moreover the previous report did not take into account the injection in fibers. A transmission of 0.9 seems reasonable toward the spectrograph. Therefore the gain in SNR is rather:

$$\frac{\mathrm{SNR_{ca}}}{\mathrm{SNR_{ma}}} = 1.5 \tag{2.2}$$

2.2.2.2 Three telescopes

Coaxial For each baseline the situation is similar to the one for two telescopes except that the flux is divided by 2.

Multiaxial The pupil configuration for the recombination is given by Fig. 2.4. Therefore the size of the pixel is $p_x = \lambda_{\min}/6D$. The scan velocity is given by the smallest baseline (1-2). It has to be the same as in the coaxial case. Therefore we will get $2N$ steps of $T/2N$ each.

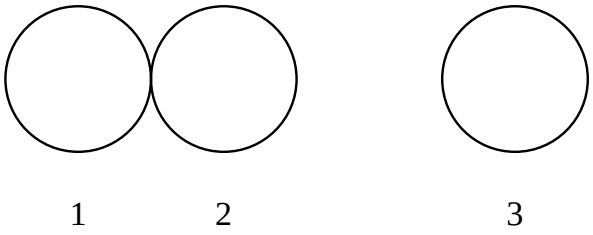

Figure 2.4: Pupil configuration for 3 telescopes in multiaxial case.

Knowing that one loses again 30% of the light due to the truncation of the Airy pattern, one gets:

Baseline 1-2. Each fringe is sampled every $\lambda_{\min}/6$ instead of $\lambda_{\min}/2$ for two telescopes. Therefore the loss in contrast is only $\mathrm{sinc}(\lambda_{\min}/6\lambda)$, i.e. 0.96.

Baseline 2-3. Each fringe is sampled every $\lambda_{\min}/3$ instead of $\lambda_{\min}/2$ for two telescopes. Therefore the loss in contrast is only $\mathrm{sinc}(\lambda_{\min}/3\lambda)$, i.e. 0.86. One also samples two fringes instead of one.

Baseline 1-3. Each fringe is sampled every $\lambda_{\min}/2$ like for two telescopes. Therefore the loss in contrast is the same, i.e. 0.72. One also samples three fringes instead of one.

The flux is spread out on 6 pixels instead of 2 pixels for 2 telescopes.

Conclusion The gain in SNR between the two configurations is then:

$$\frac{\mathrm{SNR}_{\mathrm{ca1-2}}}{\mathrm{SNR}_{\mathrm{ma1-2}}} = 1.68 \tag{2.3}$$

$$\frac{\mathrm{SNR}_{\mathrm{ca2-3}}}{\mathrm{SNR}_{\mathrm{ma2-3}}} = 1.33 \tag{2.4}$$

$$\frac{\mathrm{SNR}_{\mathrm{ca1-3}}}{\mathrm{SNR}_{\mathrm{ma1-3}}} = 1.29 \tag{2.5}$$

$$\tag{2.6}$$

2.3 Discussion

We discuss here the advantages and the disadvantages of either the coaxial recombination scheme or the multiaxial one.

2.3.1 Signal to noise ratios

In the cophasing mode, the SNR is about the same except for the loss of 30% of the light in the multiaxial configuration.

The previous chapter shows that the SNR is better with a factor 1.5 in the coaxial recombination when the instrument is in coherencing mode and scans the entire interferogram.

2.3.2 Field of view

In the high precision visibility mode, one uses fibers for spatial filtering. Therefore the field of view is limited to the Airy size of the telescope.

In imaging mode, by suppressing the spatial filter, increasing the pixel sampling of the input pupil and stretching away the subpupils, one increases the field of view of the interferometer in the multiaxial configuration. The field of view is then the unvignetted field of view of the beam in the laboratory, i.e. at least $2''$. One can not do this with the coaxial configuration because of the presence of fibers to feed the spectrograph.

2.3.3 Visibility calibration

The calibration of the visibility is given by the quality of spatial filtering and the quality of the instrument stability behind the spatial filter. A stability better than 1% in intensity gives an accuracy better than 10^{-4} in visibility.

If spatial filtering is done by pinholes, then the multiaxial configuration might be sensitive to uncorrected tilted beams in entrance and changes the ratio between the measured photometry and the actual photometry in the interferometric channel. This does not happen in coaxial recombination. If spatial filtering is done with single-mode optical fibers, the two configurations should lead to the same visibility accuracy in the long exposure mode. When in coherencing mode or in blind mode, the coaxial scheme is more natural since fast scans allow high quality visibility calibration, as demonstrated by past or existing instruments working in this mode [7]. The multiaxial scheme requires some extra calibrations due to the windowing effect by the Airy pattern or by the fiber mode profile. This has not been experimented yet.

Spatial filters made of optical fibers are therefore recommended for the high precision visibility mode.

2.3.4 Wavelength coverage

In coaxial configuration, the wavelength coverage is limited by the wavelength coverage of the fibers feeding the spectrograph. One needs 3 sets of fibers depending on the spectral band: K, $1 - 1.8$ μm, $0.6 - 1$ μm.

With the multiaxial configuration, large wavelength coverage corresponding to the spectral sensitivity of the detector can be achieved. The spatial filter has to be removed or adapted to the shortest wavelength. Differential interferometry can therefore be done for example between 1 and 2.5 μm.

2.3.5 Number of baselines

Coaxial recombination is rather simple with one baseline. The complexity increases every time a telescope is added. A configuration with 4 telescopes becomes rather complex.

Multiaxial recombination consists in adding more subpupils in a line with no redundancies. Going from 2 to 4 is rather simple, except that the anamorphous factor has to be adapted.

2.3.6 Spectral resolution

To achieve high spectral resolution, one needs to sample the spectrum. Therefore the number of pixels orthogonally to the fringes has to be doubled both for multiaxial and coaxial configuration.

Table 2.1: Comparison of the recombination schemes.

Instrument modes	Multiaxial	Coaxial
Imaging	++	
High Precision Visibility		+
High spectral resolution	+	

2.3.7 Expertise

The expertise on the two configuration types is achieved in Europe by two groups: FLUOR group for the coaxial recombination and GI2T group for the multiaxial recombination. Other interferometers in the world use mainly coaxial configuration.

The experience from the FLUOR experiment is directed on the high accuracy of the visibilities. The experience of GI2T is focused on imaging, large field of view and high spectral resolution. Therefore it is difficult to decide from these experiments since they are not comparable on the same issues.

2.4 Conclusion

The conclusion of this working group is based on criteria allowing the full use of the instrument in the three modes: imaging, high precision visibilities and high spectral resolution. Coaxial recombination has the advantage of the experience of high precision visibilities and a small gain in signal. Multiaxial recombination has advantages in imaging mode and high spectral resolution.

The multiaxial recombination scheme seems to have more operating flexibilities than the coaxial recombination scheme. However our group is not certain that it will comply with the 10^{-4} accuracy specification for visibilities in the high precision visibility mode. Normally the use of fiber-made spatial filters should allow this, but we have no experience. We however recommend the multiaxial scheme, but if the system study shows a problem, the coaxial scheme would then be preferred.

Chapter 3

Instrument subsystems

In this chapter, we describe the subsystems that form the instrument. We have followed the functional analysis done in a previous report [6].

In order to measure the beam coherence in the instrument, one has to perform the following functions:

- size adaptation of the incoming beam
- field inversion (not mandatory)
- wavefront correction
- differential refraction compensation
- control and analysis of polarization states
- optical path compensation (from atmospheric piston)
- spatial filtering
- exploration of the optical path difference
- extraction of photometric calibration
- beam combination and modulation
- spectral dispersion
- detection
- calibration and alignment

These functions are not sequentially ordered and do not correspond physically to a piece of hardware in the instrument. One subsystem can realize several functions (cf. Fig. 3.1).

3.1 VLTI interface

Interfacing with the VLTI can be done in two different ways. The proposed scheme of the VLTI Control Software (VLTICS) [8] shows a general VLTI user interface, which gives commands to the VLTICS. The VLTICS itself is sending high level commands to the beam combiner instrument. This means that the user interface is built by ESO and the beam combiner instrument's interface has to comply with ESO's rules.

However since the instrument is a rather complex module that the user could wish to control directly, the user interface can be attached directly to the instrument. This way the user sends commands to the VLTICS via LAN and an interface that has to comply with ESO's rules and directly to the beam combiner via another interface which has to be defined.

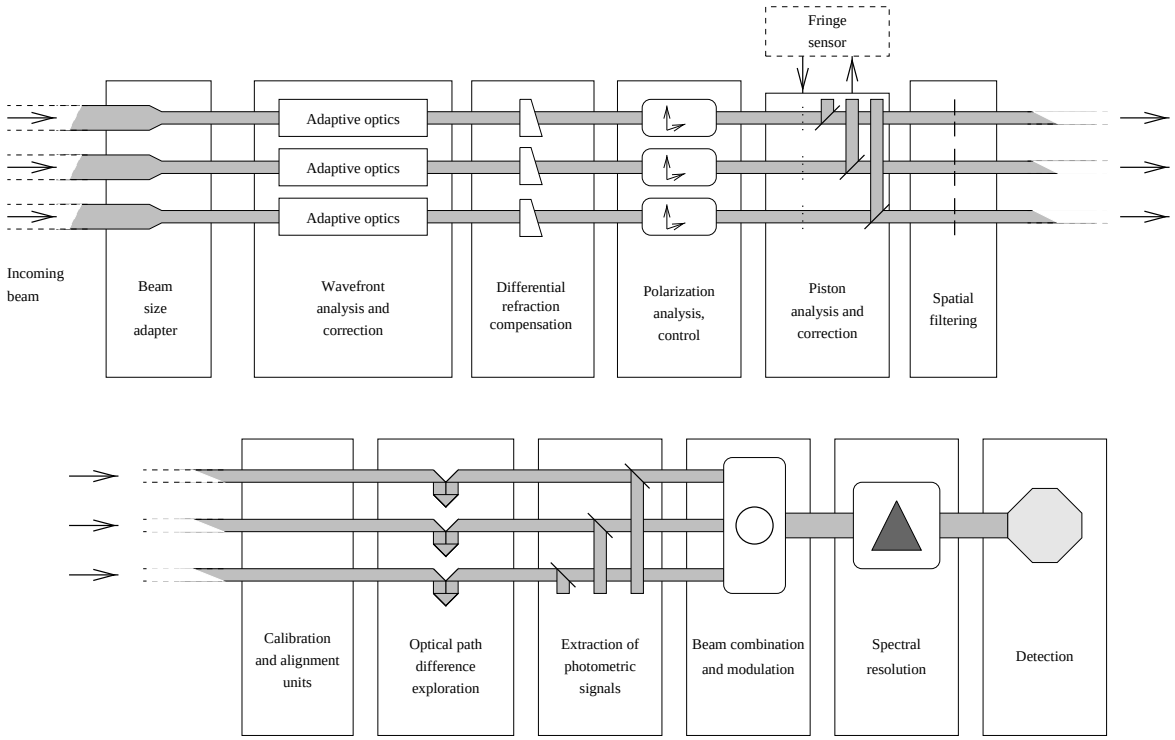

Figure 3.1: Functional diagram of the instrument.

Parts of the data exchange between the beam combiner instrument and the VLTI ask for high speed. This is not possible with communication via the LAN. To ensure this high speed communication it is necessary to have a Fast Link between the controlling device and the part of the VLTI that is controlled. A first application of this Fast Link is the data exchange between the Fringe Sensor Unit and the Delay Lines.

Another interface may be also necessary to link this instrument to other VLTI instruments (cf. section 1.4). It may be possible to use it as a fringe tracker for the phase referencing instrument or the mid infrared instrument.

The modules to which the instrument will have to dialog are:

- telescopes (pointing, source acquisition)
- delay lines (tracking)
- internal/external reference sources (optical alignment)
- double feed (external fringe tracking)
- optics/pupil stabilization (req. $\lesssim 1\%$, or $\approx 100\mu$m)
- AO (modal control, seeing and coherence time estimates)
- communications (general VLT database)

In the current scheme, adaptive optics and fringe sensor are part of the instrument itself (cf. § 3.3). Depending on the decisions that will be made by ESO and partners, these modules will also have to be considered as separate interfaces.

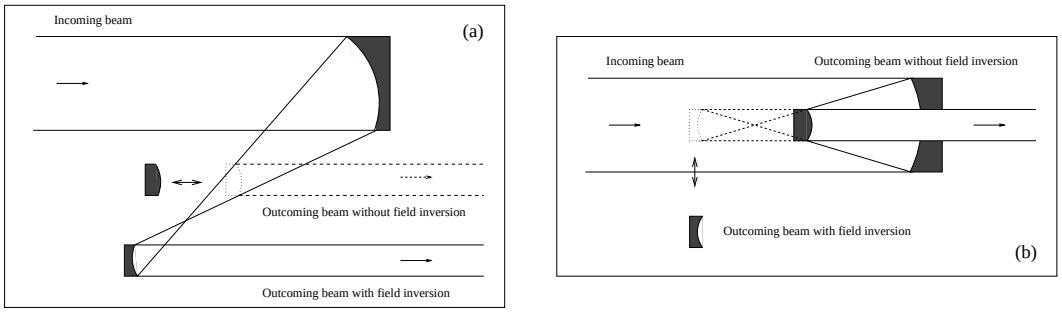

Figure 3.2: Beam size adaptation and field inversion module: a) with two paraboloids, b) with a central obscuration.

Table 3.1: Seeing conditions at Paranal.

Seeing	r_0 at 2.2μm	r_0 at 0.6μm	D/r_0 on UTs K	D/r_0 on ATs K	V
0.66″(50%)	92 cm	19 cm	8.7	1.9	9.3
0.5″(20%)	122 cm	26 cm	6.6	1.5	7

3.2 Beam size adapter and field inversion

The specifications for this module are imposed by the size of the incoming beams and the adaptive optics system. The sizes of the incoming beams will be 80 mm for the UTs and 18 mm for the ATs. The deformable mirror of the AO system has a diameter of about 50 mm.

For the beam size adaptation we propose an achromatic system consisting of a pair of mirrors. It is possible to replace the secondary divergent mirror with a secondary convergent mirror to observe in field inversion mode (cf. figure 3.2).

The beam size adaptation for the spectrograph will be done by the spatial filter subsystem since it needs to create a focal plane.

3.3 Adaptive optics

The incoming beams are disturbed by the propagation in the atmosphere. The wavefronts are distorted on spatial scales r_0 which depend on the wavelength and on meteorological conditions. The usual Paranal conditions [9] have given the results put in Table 3.1.

The characteristics of the system which is proposed are the following:

- Bimorph deformable mirror with 31 actuators from CILAS.
- Curvature wavefront sensing with 31 APDs in the visible.
- Tip-tilt is achieved with M8 mirror.
- Modulation of the wavefront sensor will work between 1 and 5 kHz. The bandwidth will be approximatively 250 Hz.
- modal optimization of the commands.

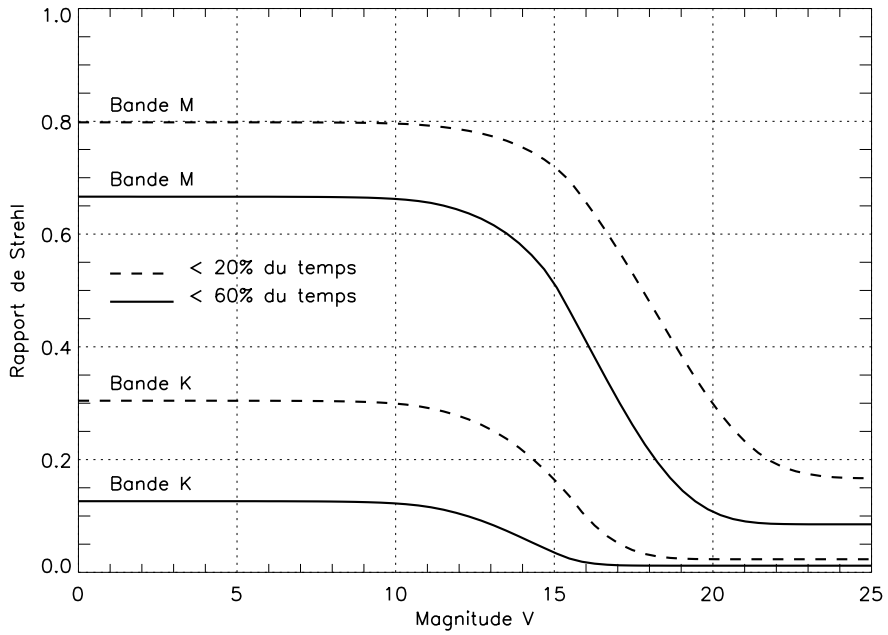

Figure 3.3: Strehl ratio for one UT (8 m), in two seeing conditions (solid line: 20% of the time, dashed line: 60% of the time

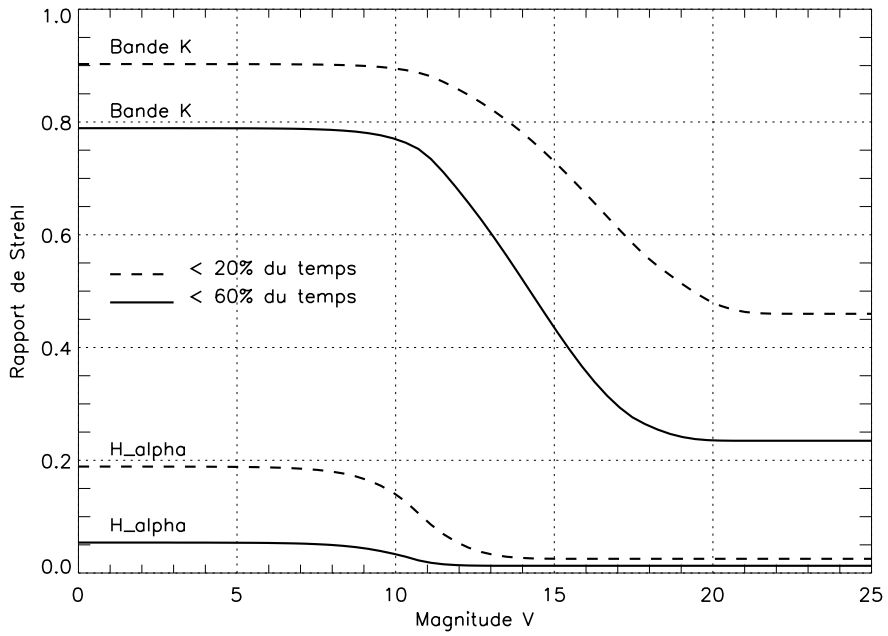

Figure 3.4: Strehl ratio for one AT (1.8 m), in two seeing conditions (solid line: 20% of the time, dashed line: 60% of the time)

Table 3.2: Gain in limiting magnitude for the PFSU.

Exp. time 23(ms)	Band-width (Hz)	Noise Power (W)	Noise Energy e^-	PICNIC magnitude gain (Δm)	Limiting H magnitude 40 Hz InSb	adapted InSb	18 e^- PICNIC
4	40	8.85×10^{-15}	294	3.0	6	6	9
8	20	6.26×10^{-15}	415	3.4	7.5	7.9	10.9
15	11	4.57×10^{-15}	567	3.8	8.5	9.2	12.3
25	6.4	3.54×10^{-15}	734	4.0	9.3	10.3	13.3

Very good evaluations of adaptive optics have already been made [6]. They give the curves of Figs. 3.3 and 3.4.

Increasing the number of actuators will not change the position of the limiting magnitude, but will increase the Strehl ratio for bright stars. To define a limiting magnitude is rather difficult since it depends on the value of the Strehl ratio limit. For example, ATs in excellent conditions of seeing give a Strehl ratio better than 0.45 for any magnitude because r_0 is of the order of the telescope diameter. If we define the required Strehl ratio to be better than 0.3 for ATs then the limiting magnitude is $V = 16.9$ in median conditions. For UTs in excellent conditions the magnitude is $V = 14.3$ with a Strehl ratio of 0.2. In median conditions, the limiting magnitude is $V = 12.2$ for 0.1 Strehl ratio.

For relatively bright stars, Strehl ratio is better than 0.8 on ATs and around 0.2 on UTs. It means that collecting power on UTs is 5 times more important than on ATs.

3.4 Fringe sensor

The focal instrument must have a fringe tracking capacity, for medium or high spectral resolution observations. Since each telescope will be able to feed the delay line with two beams, one for a bright reference star and the second one for a fainter science target, it would be particularly interesting to be able to feed the fringe sensor indifferently with the reference or the science beam.

The Prototype of Fringe Sensor Unit (PFSU) OCA is currently building for ESO has InSb detectors filtered at 40 Hz but read at 4 Khz. The measured piston is delivered at a 1 Khz frequency. The high sampling and output rates were requested by ESO for an optimization of the servo loop containing the FSU and the Delay Line. In the case of InSb detectors the SNR is affected only by the filter bandwidth. If we replace the InSb detectors by pixels of a PICNIC array, the elementary exposure time corresponding to the 40 Hz bandwidth will be of about 4 ms (as far as fringe sensing is concerned). This corresponds to a fringe scan time of 16 ms. Realistic piston simulation made in Sect. 5.1 show that under average conditions, the RMS fringe displacement over 16 ms is of $\lambda/40$, yielding a 0.1% contrast drop. This is a quite severe specification, which can be relaxed for some applications. The following table shows the gain in limiting magnitude which can be expected by using a PICNIC with 18 e^- readout noise instead of the InSb with 1.4×10^{-15} W/Hz$^{1/2}$ currently purchased for the PFSU.

The exposure times in column 1 of Table 3.2 result from Sect. 5.1 piston simulation. The limiting H magnitudes for an InSb with a 40 Hz filter, in column 6, are extracted from Fig. 5.7 of the preliminary report [6]. The figure is an approximation valid for the ATs and the UTs

within the best 20% seeing conditions. For the UTs and the best 60% seeing limit, it is necessary to subtract 1.2 magnitudes.

Our proposition is to integrate the ESO FSU in the focal instrument after replacing the InSb detectors by the best possible array. The exposure times will be adjusted according to seeing conditions and scientific program requirements. Expertise in applications requiring fast readout of small areas of an IR array is already available [15]. The effect of the slow output rate on the servo loop must be studied. One possible solution might be to build a 4 Khz signal from the much slower detector readouts with some kind of extrapolative filter.

3.5 Beam quality control

3.5.1 Spatial filtering

Spatial filtering can be achieved either by placing a pin-hole – whose size is that of an Airy disk – at a focal point, or by injecting the beam in a single-mode fiber. The main advantage of first technique is that it is simple to build and that the spatial filter can be easily removed to allow for wide field of view observations when needed, in a future version of the instrument. But it has two main drawbacks that can be overcome with a single mode fiber. First, the size of the pin-hole linearly depends upon the wavelength of observation. This is problematic for wide-band observations. In this case, to filter all wavelengths, the pin-hole size is given by the shortest wavelength, and the longer the wavelength in the spectral band, the more it is attenuated. Second, because the electromagnetic field can propagate freely after it has been filtered, a residual atmospheric tip-tilt is not filtered by the device preventing accurate visibility calibrations. It is consequently needed to servo the beam after the spatial filter to maintain optimum interferences. If, instead, a single mode fiber is used to achieve filtering, the coupling is, to a good level of approximation, achromatic since the radius of the mode is proportional to wavelength. Besides, since the field can only propagate parallel to the axis of the fiber, the direction of the beam after filtering is constant and the quality of interferences is optimum.

The chromaticity of the coupling with a pin-hole or a fiber is of prime concern since the instrument is required to be used in a range of several photometric bands from the R to the K or L band. In the hypothesis of the use of a pin-hole, a wide range of pin-hole sizes are necessary to cover this wide band. If the filter is a fiber, a different fiber is needed for each octave of wavelength. To cover the whole range, it is necessary to use three different fibers.

3.5.2 Photometric calibration

In a perfect single mode instrument using perfect spatial filters, atmospheric phase fluctuations are traded against photometric fluctuations. Photometric fluctuations induce variations of fringe contrast because of the unbalanced photometry of the interfering beams. These fluctuations can be monitored by sampling part of the beams before they are recombined. Coudé et al. (1997) [7] have shown that this is important to get good visibilities. Perrin [12] and Perrin et al. (1997a, 1997b) [13, 14] have demonstrated that this method leads to very accurately calibrated visibilities and that no bias larger than 0.3% is present in the data.

It is important to have in mind that a precise photometric calibration requires a long sequence of signal (typically one or more coherence times). As a matter of fact, it is necessary to calibrate the instantaneous photometric transmission parameters of the whole system. To

do this, the method used in Coudé et al. (1997) [7] is based on the least square method. The low frequency part of the interferograms is fitted by a linear combination of the photometric signals measured for each beam. This yields the relative gains in the two photometric channels. In practice, 100 μm long scans in K are sufficient to provide a good accuracy on visibilities. When the interferometric array is cophased it is possible to integrate the interferometric signals. The instantaneous gains calibration is lost. It is probably possible to replace it by an average calibration of the gains. That will induce a decrease of visibility accuracy. But the magnitude of this effect has not yet been determined. It may be negligible but this is not sure and it depends upon what accuracy is mandatory, given a scientific program.

It is not necessary to spectrally analyze the photometric signals since rapid spectral variations can be neglected relative to mean photometric variations. Besides, the detection of photometric signals can be performed with the same detector as the one used for interferometric signals.

3.5.3 Polarization control

Although it is possible, in theory, to feed the instrument with beams of equal polarizations as long as they undergo reflections on mirrors with the same series of direction cosines, it is not realistic to rely on theoretical anticipations since it is far from being guaranteed that all the mirrors have strictly identical coatings. The consequence is that the instrumental contrast is degraded because the s and p polarizations are differentially rotated between the interfering beams and delayed.

Despite this is the concern of ESO to deliver equally polarized beams to the combiner, it is safer to include a facility to control polarizations in the instrument. The control can be achieved either with a Babinet prism or the equivalent device with fibers. This method has proved to be efficient when the contrast is directly optimized on an astronomical source on the sky. It allows to reach instrumental contrasts as high as 95% [12].

3.5.4 Differential refraction compensation

Because the atmosphere is equivalent to a prism, incident beams of different wavelengths are seen to come from slightly different directions. Since the instrument is supposed to cover a wide range of photometric bands in the long term, refraction will have to be compensated otherwise the quality of the optical alignment will be both wavelength and zenithal distance dependent. But it will also be necessary to compensate for refraction within a photometric band when observing with unit telescopes because differential refraction between one side of the band to the other amounts to a good fraction of an Airy disk both in the visible and in the near infrared. If not corrected, differential refraction will thus induce bad coupling with the spatial filter for wide band observations.

3.6 Beam combiner

All of the characteristics of the beam combiner has already been reviewed in chapter 2.

The flat mirrors R1, R2, R3 (diameter 40 mm) are spaced in order to produce beams with the most compact non redundant spacing. The two cylindrical mirrors C1 and C2 are combined in an afocal system which expands the image in the fringe direction (perpendicularly

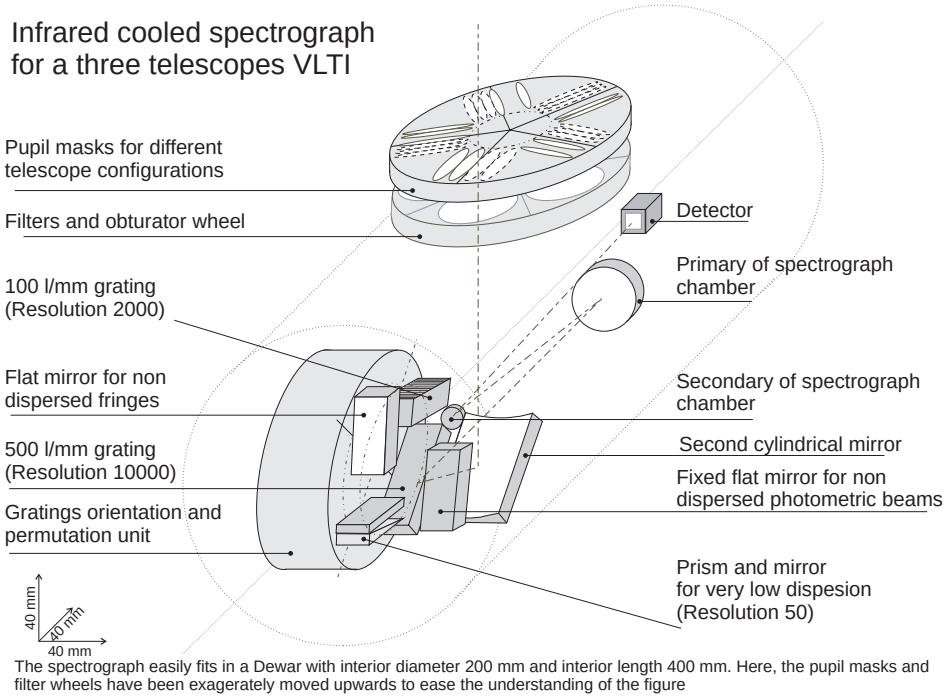

Figure 3.5: Cooled infrared spectrograph for the AMBER instrument.

to the dispersion). In the dispersion direction C1 and C2 behave as flat mirrors and have no effect. The anamorphosis factor is given by the ratio of the focals. Typical values are:

- C1: height=40 mm, length=160 mm, focal=1000 mm
- C2: height=40 mm, length=20 mm, focal=100 mm

3.7 Spectrograph

The maximum resolution desired in K is 10000. The maximum number of lines per mm usable in K is about 500 l/mm and a 40 mm grating is needed for a 10000 resolution considering an equivalent width of $2\lambda/D$ for the spatial filter in the dispersion direction. This sets the beam diameter. Combining the dispersion of the grating and the size of the detector pixels 40 μm gives a chamber focal length of 800 mm. To decrease the size of the spectrograph, the chamber contains two off-axis mirrors (Ch1 and Ch2) whose combination has an equivalent focal length of 800 mm. It is then possible to include the spectrograph inside a cryostat with interior diameter 200 mm and length 400 mm.

The resolutions will be $10000, 2000, 50$ and 0. The first two will be obtained with 500 l/mm and 100 l/mm gratings, the third with the prism and the last with a flat mirror.

3.8 Detector

Because of the many different approaches to fringe detection required by the several observing modes, the control of the detector is best seen as an independent subsystem. The detector

itself will be of the PICNIC type, sensitive in the range 1 to 2.5μm, with 256×256 pixels of 40 μm and RON $\lesssim$20 e$^-$. The main feature of this detector is the ability to perform fast read–out of selected rows and columns, which is a necessary requirement when dealing with fast data flows. The peak data rate in the most demanding mode (fast acquisitions of dispersed spectra along several lines of pixels) is estimated to be $\approx$0.6–1Mb/s. Such data rates can be effectively dealt with in subarray mode, as has been shown by an application implemented on a NICMOS array [15] and under further development at the Arcetri Observatory. In particular, in addition to the sheer read–out speed, it is important to achieve flexibility in the selection of the individual pixels and lines. Consider for instance the constraints imposed by spectral resolution as opposed to broad–band, by 2 and 3 telescopes recombination schemes, by the photometric control channels, by the polarimetric mode.

Due to the high data rate, the raw data storage should be implemented in the most direct way, from the detector electronics directly to the disks and tapes that form the acquisition subsystem (see next section and Fig. 3.6). Those subsystems that will also need access to the raw data (such as the so–called quick look monitor, the VLTI database, etc.) can do so at lower priority through the LAN.

3.9 Instrument control

The control of the instrument is one subsystem by itself. As a matter of fact, the user must be able to control the different subsystems thanks to high level commands. We suggest the diagram of Fig. 3.6 as a general scheme for instrument control, where the interface with the VLTI (ESO side) is well separated from the instrument subsystems. In this approach, we have not dealt with the actual details and rules of the ESO VLTI control software (VLTICS). It is clear that a practical implementation will require a thorough study, preferably in close cooperation with experts from ESO. However, this simple sketch highlights some of our ideas conveniently. In particular, we envision that the user should be able to work from a master WS by means of a graphical user interface (GUI) that should enable him/her to send commands to/from the VLTICS by means of a LCU module, and program the steps required on the instrument side for the actual observation (sequencer module). The user should be able to control directly some subsystems (such as the FSU, the AO, etc.). Observing procedures are defined as sequences of commands to the different subsystems. Subsystems dialog via on-line database.

Also, we have estimated that the actual data acquisition will represent a critical task for this software, due to the large volume of data that may be expected at least under some observing modes. The data flow from the detector (PICNIC module) to the data storage devices (disks and DATs or equivalent) should be as fast as possible. These devices should be accessible also by a powerful workstation that will enable the user to analyze the data almost in real–time, by running a subset of the actual data reduction package on the data being acquired. This preliminary reduction is essential, in order to give the user a feeling of the progress of the observation and choose the next moves. Also essential is the availability of what we have called a quick–look program. This latter should run automatically on a separate monitor WS, where the user can observe the progress of a number of selected quantities (such as for instance seeing, visibility, fringe tracking error, etc.). Given the nature of interferometric observations, where the final information is deeply embedded in the data, such a tool is of paramount importance to give the user a feeling of the quality of the data being collected.

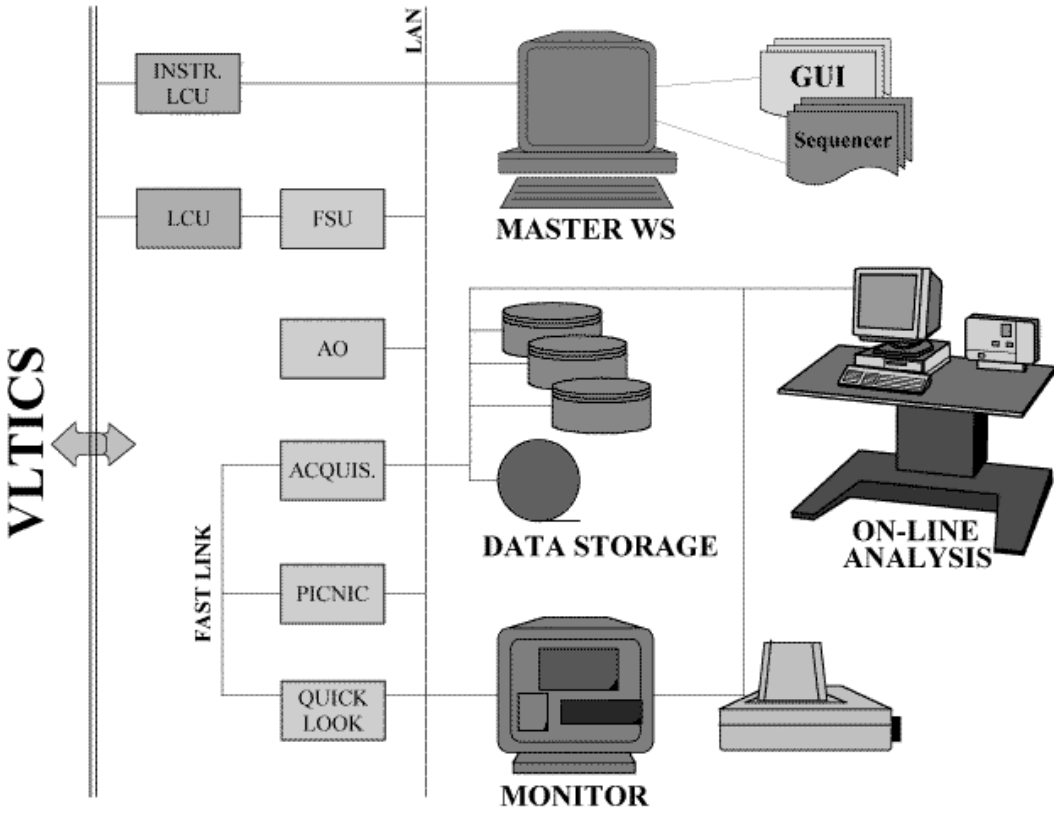

Figure 3.6: General outline of the instrument control.

Chapter 4

Observing procedures and data reduction

4.1 Calibrating procedures

4.1.1 Optical alignment

The alignment of the interferometer is a procedure whose aim is to allow the detection of fringes with an optimum signal to noise ratio. It can be divided in four steps:

1. alignment of the interferometer optics;
2. matching of the interferometer and telescopes optical axes;
3. calibration of the internal metrology;
4. optimization of the instrumental transfer function.

In the first step, all the optics of the interferometer are internally aligned from the beam combiner up to mirrors located as close as possible to the primary mirrors of the telescopes. After this step, the beam combiner is aligned and the instrument optical axes have been internally defined. At this stage, the instrument optical axes do not necessarily match those of the telescopes. This is achieved, in the second step, by centering the entrance pupils with respect to the optical axes with pupil plane mirrors. The centering of the image plane is supposed to be achieved with the adaptive optics control loop. The third step is explained further in this report. The last step was addressed before. The first step (internal alignment) requires an internal source. The most convenient location for the injection of the internal source in the instrument is the recombination point. Corner cubes can be placed, in each beam, as close as possible to the entrance pupils. These corner cubes can be the cube corner mirrors located on M2. The fine adjustment of the optics is obtained by injecting the source at the recombination point and by superimposing the direct beams with the retroreflected beams. Step two, instead, is realized with a natural star on the sky.

4.1.2 OPD calibration

From an experimental point of view, it is difficult to guess the internal delay between the beams because of the cumulated uncertainties on the location of each optical element. We thus

recommend that the internal metrology of the instrument be calibrated by self-collimating the array. A source can be injected at the recombination point of the array. The beams are then retro-reflected by corner cubes located at the center of M2. Fringes are detected when the optical paths are equalized in all arms of the interferometer, yielding the differential distances between the recombination point and the secondary mirrors of the telescopes. To achieve a full calibration of the internal OPDs remains the measurement of the distance between the secondary mirrors and the primary mirrors of each telescope. These should be accurate to better than a centimeter.

4.1.3 Visibility calibration

We assume that the only loss of coherence that needs to be calibrated is the instrumental loss of coherence (polarization, detector response, etc) and that no bias is introduced by the fringe detection scheme. The contrast measured on the scientific source is calibrated by comparing it to the contrast measured on a calibrator star whose visibility is known. The calibrator may be an unresolved source or a well calibrated source, the accuracy on the final estimate of the module of the visibility of the scientific source will depend upon the good knowledge of the calibrator. The criteria to select the calibrator vary from one estimator to another. Nevertheless, since visibility estimators are chromatic, it is necessary that the source and the calibrator have similar spectral types. Polarization effects vary with the inclination of the beams on the mirrors hence with the position of sources on the sky. It is thus necessary to use calibrators that are close to the target sources. In particular, a very accurate calibration will be achieved if the beams are stabilized in the instrument both in image and pupil planes. This will ensure that the beams will impact mirrors at constant locations, preventing contrast fluctuations created by spatial inhomogeneities of the surface of mirrors. It is also necessary that the observation of the target source and of the selected reference happen at close instants to avoid biases in the data due to possible time-dependent variations of the instrumental transfer function.

4.1.4 Phase closure

Theoretically, phase closures are self-calibrated. Nevertheless, to be scientifically acceptable, it is necessary to compare phase closures measured on an unresolved source and on the scientific source. This will yield the level of confidence in phase closure measurements achieved by the instrument and the attached uncertainty. The unresolved source used for the calibration of the module of the visibility can be used as well for phase closure calibration.

4.1.5 Detector calibration

Classical detector calibrations will be needed in both wide-band and dispersed modes. Calibration of the relative response of pixels will be achieved by recording flat fields. The map of pixels response should be stable enough and allow flat field sessions to occur once per night. On the contrary, it is necessary to alternate dark current maps and data acquisition. As a matter of fact, quadratic visibility estimators require the computation of the power spectral density of detector noise. Besides, dark current maps will have to be acquired with the same elementary exposure time as the fringe signal to avoid bias by non linearities.

4.1.6 Spectrograph calibration

Spectral resolution will only be devoted to the analysis of the combined beams. Photometric signals will be acquired in wide band. The parts of the beams collected by the apertures and pertaining to the Earth atmosphere will not build interferences because they are basically incoherent. Therefore, no telluric lines will be detected by the spectrograph. As a consequence, the spectrograph will be calibrated using lamps that are internal to the instrument.

4.2 Software

There are different software packages for observation preparation, observation control, and data reduction that have to be developed. Some of the work has to be discussed together with the VLTI data analysis group.

4.2.1 Observation preparation

This package helps the user to prepare his observations. It includes selection of object, telescopes, observation mode, integration time, spectral resolution, etc. These selections allow the program to give the observer rough estimates on expected performance of the interferometer, especially in accuracy and sensitivity.

4.2.2 Data simulation

When using the interferometer at its' limits or when he/she just wants to see what he/she can expect from the interferometer, the observer should use this program. Similar to programs used with radio interferometers (like `fake` used with VLBI) the user can model his source, with estimated flux, apparent morphology, coordinates and the like, select the interferometer's mode, and retrieve an image as seen by the interferometer. This enables the observer to select the best observational modes, the correct integration time, or just the feasibility of his proposal.

4.2.3 Instrument master and observing package

This package represents the software that masters the instrument and the general user interface (GUI). It enables the user to control the beam combination instrument and the VLTI to perform according to his observation scheme. It also monitors the status of the experiment and delivers this status to the recording unit for data header management. Furthermore there must be the possibility to search object catalogues, especially for calibrating procedures.

4.2.4 Monitoring

This package is running on a computer which sees the continuous data stream coming from the beam combination detector. There are various tasks running simultaneously, as display of raw data, integration of raw data, computation of visibility and so on. These tasks depend on the operation mode of the interferometer and enable the user to see the interferometer's performance on-line. Only a minimum interaction of the user is required. Furthermore also quantities as the instance seeing, given by the AO system, or the fringe tracking error, given

by the FSU, will be monitored. It runs in real time, on a workstation or maybe a DSP system, aiming more on speed than accuracy.

4.2.5 On-line analysis

This software enables the user to perform all the data reduction procedures he needs to retrieve information on the observed object. It contains the complete set of algorithms that are used in the standard data reduction pipeline described in the two following points. For on-line purposes short cuts in the data reduction process may be necessary to speed procedures up. The software runs on a workstation with direct access to the data acquisition medium.

4.2.6 Visibility and spectra reduction

Within this package the observer finds all the software which is used to reduce the raw data to obtain visibilities and/or phase information in imaging and spectroscopic mode. It contains all calibration procedures and information retrieval algorithms for the different observational modes of the beam combination instrument.

4.2.7 Image reconstruction

This software is designed to compute the final images and spectra. We hope we can rely on the expertise which is available in the radio interferometry community. Most of the existing algorithms should be applicable for our needs.

Chapter 5

Anticipated performance

We present an estimation of the performance of the instrument. First we show the results of piston simulation for two UTs. Then we compute the anticipated performance of the instrument in its three modes. Finally we present a rule of thumb from the performance of current interferometers to check that the numbers we give are correct.

5.1 Piston variation

The fringes will not be stable in the instrument. They will move due to the atmospheric piston. We have applied the formulation given by Perrin (1997) [11] to the VLTI, with the following numbers :

- Baselength: 40 m
- Wavelength: 2.2 μm
- Aperture diameter: 8 m
- Fried parameter: 60 cm
- Wind speed: 20 m/s

The model assumes that the outer scale of turbulence is larger than the baseline. Figure 5.1 shows the value of piston standard variation in function of temporal sequence length. Table 5.1 gives some typical numbers.

These results are intuitive. An 8 m telescope filters out the variation of atmospheric piston on time scale smaller than 0.4 s (D/v). The time scale for ATs is rather like 0.1 s. This gives us interesting results: piston is smaller than $\lambda/10$ for an exposure time less than 150 ms leading to a contrast loss below 1.6%. To achieve less than 10^{-4} loss in contrast, one needs to have piston effect less than $\lambda/130$, i.e. an exposure time less than 50 ms.

Table 5.1: Values of piston standard deviation for different sequence length in fringe units at 2.2 μm.

Time	1 ms	10 ms	100 ms	1 s	10 s
UTs (λ)	10^{-6}	3×10^{-4}	0.04	2.7	11.2
ATs (λ)	10^{-5}	2×10^{-3}	0.21	3.5	11.3

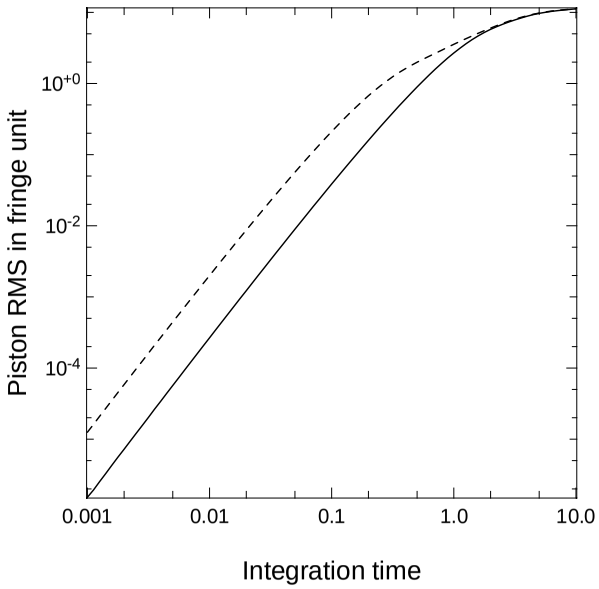

Figure 5.1: Piston standard deviation in function of the temporal sequence length (solid line: UTs, dashed line: ATs)

5.2 Limiting magnitudes

We have calculated the limiting magnitudes in the three different modes. The following characteristics of the VLTI have been chosen. The previous report [6] justifies all these numbers.

- *Telescope diameter :* $D = 8$ m for the UTs, $D = 1.8$ m for the ATs;
- *Global optical transmission for VLTI + instrument:*
  K band: $t = 7 \times 10^{-3}$ for the UTs, $t = 0.03$ for the ATs;
  H band: $t = 1.5 \times 10^{-3}$ for the UTs, $t = 0.01$ for the ATs;
  J band: $t = 5 \times 10^{-4}$ for the UTs, $t = 5 \times 10^{-3}$ for the ATs;
- *Number of measurements needed for one visibility measurement:* $n = 4$ for 2 telescopes and $n = 12$ for 3 telescopes ;
- *Detector read-out noise:* $\sigma_d = 18$ e$^-$;
- *Detector quantum efficiency :* $\eta = 0.5$;

The spectrograph is cooled down to 77K and therefore the thermal background is negligible. One takes a SNR = 5 for the definition of the limiting magnitude. The SNR formula is then for a photometric limiting magnitude:

$$SNR = \frac{N_*}{\sqrt{\sigma_*^2 + \sigma_d^2}} \tag{5.1}$$

Knowing the read-out noise σ_d and the photon noise $\sigma_* = \sqrt{N_*}$, we find that the number of photo-electrons at the limiting magnitude is $N_L = 104$. The limiting magnitudes are then defined by:

$$m = 2.5 \log \left(\frac{E_0 \, S \, t \, \lambda / R \, \tau \, \eta}{N_L \, n \, hc/\lambda} \right) \tag{5.2}$$

Table 5.2: Limiting magnitudes of the instrument.

	Imaging mode			*High Precision Visibility mode*		
	J	H	K	J	H	K
2 UTs	10.6	11.3	12.8	8.1	8.8	10.3
2 ATs	8.8	9.1	10.1	7.3	7.6	8.6

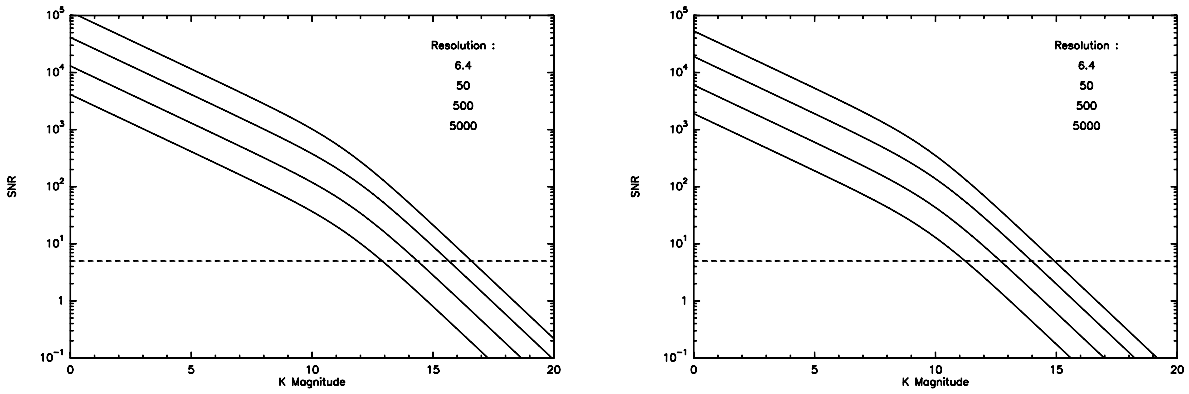

Figure 5.2: Signal to noise ratios in K band for the UTs (left) and the ATs (right) in High Spectral Resolution mode ($\tau = 100$ s).

The limiting magnitudes in the different instrument modes are discussed in the following subsections.

5.2.1 Imaging mode

The precision in visibility must be better than 10^{-2}, i.e. a fringe stabilization better than $\lambda/15$. With the UTs, $\tau = 100$ ms gives a fringe stabilization of the order of $\lambda/25$. With the ATs, $\tau = 40$ ms gives the same precision. We have used these exposure times to compute the limiting magnitudes reported in Table 5.2.

5.2.2 High Precision Visibility mode

The precision in visibility must be better than 10^{-4}, i.e. a fringe stabilization better than $\lambda/130$. An exposure time of $\tau = 10$ ms gives almost 40 times higher accuracy for the UTs and 5 times higher accuracy for the ATs. We have therefore used $\tau = 10$ ms as the basic exposure times with the UTs and ATs in Table 5.2.

5.2.3 High Spectral Resolution mode

In High Spectral Resolution mode, the stars are bright enough so that we can fringe track on the stars themselves. Therefore the integration time in the spectral channel can be as long as desirable providing that it is short compared to baseline variations. We think that $\tau = 100$ s is a basic number for this mode. The limiting magnitude has no useful meaning. We prefer to present SNR curves for different resolutions on Fig. 5.2.

5.3 Comparison with existing facilities

In this section, we want to show that the previous estimations are realistic when compared to the current performance of existing infrared interferometers like IOTA or PTI.

On IOTA, the siderostat diameters are 0.45 cm. In K band with a tip-tilt correction, we estimate that the Strehl ratio is 0.7 compared to a Strehl ratio of 0.2 on UTs. Therefore, the gain from going from IOTA siderostats to UTs is $(800/45)^2 \times 0.2/0.7 = 90$. The integration time on IOTA is generally $\tau = 3$ ms. We assume that the optical throughput is equivalent even if for the VLTI it will probably be worse than for IOTA. The detector used for IOTA is a NICMOS3 with 10 e^- read-out noise and the Wyoming table succeeded to acquire fringes on a star with K magnitude between 5 and 6. Therefore with these numbers, we find that VLTI limiting magnitude in imaging mode should be approximatively between 13 and 14, and in high precision visibility mode between 10.5 and 11.5.

The numbers for PTI are very similar to the one given for IOTA, except that the integration time is rather like $\tau = 10$ ms and the read-out noise of the NICMOS detector is 18 e^-. PTI has detected fringes on a $K = 5.5$ unresolved star. These numbers give a limiting K magnitude close to 12.9 in imaging mode and 10.4 in high precision visibility mode.

These two interferometers are not yet well optimized and should achieve better sensitivity in the near future. For example, PTI has an expected limiting magnitude between 6.8 and 7.8.

Chapter 6

Conclusion

6.1 Summary

We report the study of a focal instrument for the VLTI, AMBER, whose main characteristics are:

1. Major modes are imaging, high precision visibility and high spectral resolution corresponding respectively to the study of extended structures (AGNs, YSOs, circumstellar matter), multiple objects (binaries, exoplanets) and stellar structure.
2. The optical concepts which have been studied are based on coaxial and multiaxial recombiners. We think that the multiaxial concept presents more instrumental flexibility than the coaxial one especially for imaging and high spectral resolution modes. If the detailed system study reveals some unexpected problems, we will recommend the coaxial concept.
3. High precision visibilities will be obtained by filtering spatially the incoming beams and calibrating accurately the photometry.
4. The instrument can deal with two or three beams in entrance.
5. Operation in the near-infrared and later in the red part of the spectrum.
6. The instrument is based on experience gained in the near-infrared (spatial filtering and photometric calibration on FLUOR) and in the visible (recombination table of GI2T).
7. Adaptive optics with a low number of actuators is mandatory. Strehl ratios of 0.1-0.3 with the UTs in K band and 0.05-0.2 with the ATs in H_α.
8. Spectral resolution up to 10000.
9. Anticipated performance gives limiting magnitudes of $K = 12.8$ on the UTs and $K = 10.1$ on the ATs in the most sensitive mode.

6.2 Resources

For the moment, the resources are the ones available from the French interferometric community [6] and the ones available at the Osservatorio Astrofisico di Arcetri.

The cost of the instrument [6] is evaluated in the order of 1.2 MDM with adaptive optics included (0.6 MDM). The cost will be specified more clearly after a detailed system study.

6.3 Development strategy

We suggest to develop the instrument in two phases:

Phase A. 2-way beam combiner, adaptive optics, polarization control, spectrograph, instrument control. Date: mid-2000 when the UTs and DLs will be ready.

Phase B. 3-way beam combiner, extension toward the red. Date: 2002 when the ATs will be available.

Bibliography

[1] ISAC report, 1996, *A new start for the VLTI*, The ESO Messenger, 83

[2] Implementation Plan of ESO VLTI, Issue 2.0 Draft, 9 janvier 1997, ed. O. von der Lühe.

[3] Update of the *Agreement on the enhancement of the Very Large Telescope Interferometer with a third auxiliary telescope and delay line* from December 18, 1992, autumn 1996, between ESO, CNRS and MPG.

[4] VLT report 59b, 1989, *The VLT Interferometer Implementation Plan*, ESO/VLT Interferometry Panel, ed. J.M. Beckers

[5] VLT report 65, 1992, *Coherent combined instrumentation for the VLT Interferometer*, ESO/VLT Interferometry Panel, ed. J.M. Mariotti

[6] Coudé du Foresto V., Malbet F., Mékarnia D., Petrov R., Reynaud F., Tallon M. 1997, PNHRAA report, *Preliminary study of the near-infrared/red instrumentation of VLTI and GI2T*

[7] Coudé du Foresto, V., Ridgway, S.,Mariotti, J.-M. 1997, A&AS 121, 379-392 – *Deriving object visibilities from interferograms obtained with a fiber stellar interferometer.*

[8] VLT-SPE-ESO-15400-0886, 2.0, 18/12/96 — *VLTI Software - Requirement Specifications*

[9] Andersen, T. 1996, *Seeing Statistics at Cerro Paranal*
`http://www.hq.eso.org/vlt/systeng/environ/site.htm`

[10] Shao, M., Staelin, D.H., 1980, Applied Optics, vol. 19, 1519-1522 – *First fringe measurements with a phase-tracking stellar interferometer*

[11] Perrin G. 1997, A&AS 121, 553 – *Correction of the "piston effect" in optical astronomical interferometry.*

[12] Perrin G. 1996, PhD thesis, Université Paris 7

[13] Perrin G., Coudé du Foresto V., Ridgway S.T. et al. 1997a, Proc. "Fundamental stellar properties: the interaction between observation and theory", T. Bedding Editor, 18-21

[14] Perrin G., Coudé du Foresto V., Ridgway S.T. et al. 1997b, submitted to A&A.

[15] Richichi A., Baffa C., Calamai G., Lisi F. 1996, AJ 112, 2786 – *The TIRGO lunar occultation program: summary of the 1985-1995 observations*